



## Effect of inhomogeneous distribution of non-metallic inclusions on crack path deflection in G42CrMo4 steel at different loading rates

S. Henschel, L. Krüger

*Institute of Materials Engineering, Technische Universität Bergakademie Freiberg, Gustav-Zeuner-Str. 5, 09599 Freiberg, Germany*

*sebastian.henschel@imt.tu-freiberg.de*

**ABSTRACT.** An inhomogeneous distribution of non-metallic inclusions can result from the steel casting process. The aim of the present study was to investigate the damaging effect of an inhomogeneous distribution of non-metallic inclusions on the crack extension behavior. To this end, the fracture toughness behavior in terms of quasi-static J- $\Delta a$  curves was determined at room temperature. Additionally, dynamic fracture mechanics tests in an instrumented Charpy impact-testing machine were performed. The fracture surface of fracture mechanics specimens was analyzed by means of scanning electron microscopy.

It was shown that an inhomogeneous distribution significantly affected the path and, therefore, the plane of crack growth. Especially clusters of non-metallic inclusions with a size of up to 200  $\mu\text{m}$  exhibited a very low crack growth resistance. Due to the damaging effect of the clusters, the growing crack was strongly deflected towards the cluster. Furthermore, crack tip blunting was completely inhibited when inclusions were located at the fatigue precrack tip. Due to the large size of the non-metallic inclusion clusters, the height difference introduced by crack path deflection was significantly larger than the stretch zone height due to the crack tip blunting. However, the crack path deflection introduced by a cluster was not associated with a toughness increasing mechanism. The dynamic loading ( $\dot{K} \approx 10^5 \text{ MPam}^{0.5} \text{ s}^{-1}$ ) did not result in a transition from ductile fracture to brittle fracture. However, the crack growth resistance decreased with increased loading rate. This was attributed to the higher portion of relatively flat regions where the dimples were less distinct.

**KEYWORDS.** Non-metallic inclusions; Clusters; Crack tip blunting; Crack path deflection.

### INTRODUCTION

It is well-known that non-metallic inclusions have a detrimental effect on the deformability and toughness of metallic materials [1, 2]. As a result of the steel casting process, clustering of non-metallic inclusions can occur [3].

The damage evolution during ductile fracture consists of void nucleation, void growth and void coalescence [4]. Void nucleation is caused by failure of the particle/matrix interface or by fracture of the particle [5]. The latter mechanism is observed at relatively well-bonded inclusions. Here, cracking within the particle occurs perpendicular to the highest principal stress. The void nucleation rate increases with inclusion size but is unaffected by an increased level of stress triaxiality [6]. In contrast, void growth is accelerated by hydrostatic tensile stresses and by larger inclusions [6]. Finally, void coalescence can take place by necking of the material between the individual voids. Depending on the void size and



the relative position of different voids, void sheets can be formed [6]. This process is characterized by strain concentration in a band between voids [7]. Hence, the macroscopic strain is relatively small.

In addition to the inclusion characteristics size and volume fraction, the size distribution and, therefore, the distance distribution is an important microstructural parameter. According to [8], a uniform distribution of the formed voids leads to a minimum of strain to fracture. This result from numerical calculations is attributed to the spacing between the voids, which are relatively small in a uniform distribution. According to [8], the higher ductility of a non-uniform void distribution is explained by a suspended void coalescence. The void coalescence is suspended until sufficient void growth is achieved in the remaining material. On the other hand, a locally higher content of porosity leads to strain localization and, consequently, to fracture in this region [9].

In the transition range, an increase of loading rate results in a decrease of fracture toughness [10]. In the upper shelf regime, the opposite relation is found [10]. An increased loading rate promotes the void nucleation [11]. The void growth rate is reduced with increasing loading rate. This correlates with the increased yield strength and decreased work hardening rate at higher loading rates [11].

According to [12], strain localization is promoted in a material with inhomogeneities. The consequence of such strain localization during a dynamic fracture test is adiabatic heating in the plastic zone in front of a crack [13].

The aim of the present paper is the characterization of the damaging effect of an inhomogeneous distribution of non-metallic inclusions. To this end, crack initiation and growth was studied under conditions of quasi-static as well as dynamic loading. Clustering of non-metallic inclusions was investigated by means of fractography. Furthermore, the effect of non-metallic inclusion clusters on the formation of the crack path is discussed.

## MATERIALS AND METHODS

### *Investigated steel*

In this study, the quenched and tempered cast steel G42CrMo4 (DIN EN 10293, 1.7231) was tested. Non-metallic inclusions were intentionally added to the metallic melt. This was achieved by a "contaminating filter" in the casting gate coated with loose alumina particles. After contamination, the melt flowed through the actual metal melt filter, which was utilized to clean the melt. This cleaning filter was characterized by its functionalized surface. Information about the coating of the contaminating filter and the cleaning filter is shown in Tab. 1. Details of the filter manufacturing process can be found in [14]. The chemical composition of the casting plates is given in Tab. 2.

Cast	Contaminating filter	Cleaning filter
A	Al <sub>2</sub> O <sub>3</sub> (0–200 μm)	—
B	Al <sub>2</sub> O <sub>3</sub> (0–200 μm)	Al <sub>2</sub> O <sub>3</sub> -SiO <sub>2</sub> (Mullite)
C	Al <sub>2</sub> O <sub>3</sub> (0–200 μm)	Al <sub>2</sub> O <sub>3</sub>

Table 1: Coating of the contaminating and cleaning filter. Substrate: Al<sub>2</sub>O<sub>3</sub>-C.

Cast	C	Cr	Mo	Mn	Ni	Si	Al	S	P	Fe
A	0.41	0.90	0.24	0.78	0.21	0.53	0.09	0.007	0.011	bal.
B	0.43	0.92	0.25	0.79	0.22	0.54	0.09	0.007	0.011	bal.
C	0.42	0.98	0.25	0.80	0.22	0.53	0.09	0.009	0.018	bal.

Table 2: Chemical composition (in wt.%) of the casting plates determined by glow discharge optical emission spectroscopy.

The machined samples were austenitized at 840 °C in a vacuum, followed by quenching in a stream of He. Tempering was performed at 560 °C in a N<sub>2</sub> atmosphere. Fig. 1 shows the microstructure of the material that consisted of tempered martensite.

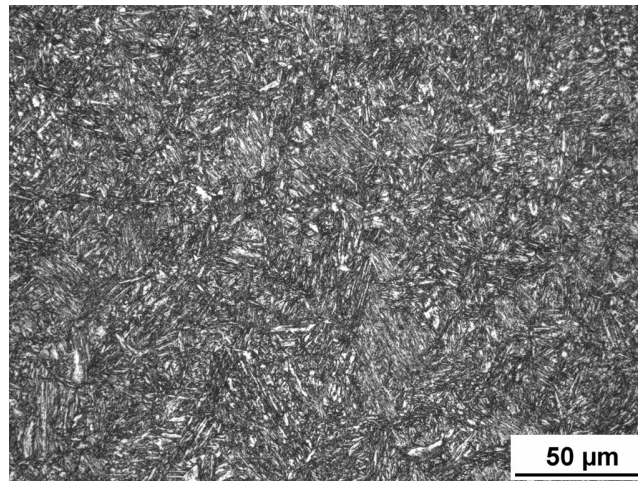


Figure 1: Microstructure of the investigated steel: tempered martensite.

The inclusion distribution was analyzed for polished cross sections utilizing the software Particle Inspector (Olympus). Small inclusions located in a group were considered as one inclusion cluster. Details of the mathematical procedure are given in a previous paper [15]. The inclusion size distribution is given in Tab. 3.

Size class ( $\mu\text{m}$ )	Cast A	Cast B	Cast C
2–5	988	1635	773
5–10	180	159	136
10–20	51	77	74
20–60	47	89	52
> 60	6	9	0

Table 3: Inclusion size distribution (inclusions/ $\text{mm}^2$ ).

### Fracture mechanics tests

The materials resistance against crack initiation and growth under quasi-static loading conditions ( $\dot{K} = 2 \text{ MPa}\sqrt{\text{m}}/\text{s}$ ) was determined according to ISO 12135 [16]. The single specimen unloading compliance technique was applied. Pre-cracked and side-grooved specimens ( $a_0/W = 0.5$ ,  $B_N/B = 0.8$ ) were tested in a servo hydraulic universal testing machine. Single edge-notched bend specimens ( $L \times W \times B = 120 \times 20 \times 10 \text{ mm}^3$ ) were loaded in three-point bending ( $S/W = 4$ ). Periodical unloadings during the test enabled the calculation of the unloading compliance from the crack opening displacement. Hence, the crack length was determined for each unloading step. The plastic part of the energy  $U_p$  was used to determine the J integral at the different stable crack extensions  $\Delta a$ :

$$J = \frac{K_I^2(1-\nu^2)}{E} + \frac{2U_p}{B_N(W-a_a)} \cdot \left(1 - \frac{\Delta a}{2(W-a_0)}\right) \quad (1)$$

Tests under dynamic loading conditions ( $\dot{K} \approx 8 \dots 9 \cdot 10^4 \text{ MPa}\sqrt{\text{m}}/\text{s}$ ) were performed in an instrumented Charpy impact-testing machine. The low-blow technique was applied. Multiple specimens ( $L \times W \times B = 55 \times 10 \times 10 \text{ mm}^3$ ) were subjected to different initial velocities of the impact tup. Hence, different amounts of stable crack extension  $\Delta a$  were achieved. The force signal was derived from the elastic deformation of the instrumented tup. The velocity and the deflection of the sample were determined by a laser system (Polytec OFV-525). This system utilizes the Doppler Effect, i.e. the frequency and phase modulation of the laser light by the velocity and the displacement, respectively, of the sample in laser beam direction. The laser beam direction was equivalent to the load line. The J integral was calculated with Eq. (1).

Irrespective of the loading rate, the final crack length after the test ( $a_f = a_0 + \Delta a$ ) was marked by heat tinting. Finally, breaking open of the specimens enabled the measurement of  $a_0$  and  $a_f$  by means of light microscopy.

### Fractography

Fracture surfaces were investigated by means of scanning electron microscopy (SEM) with secondary electron contrast and energy dispersive X-ray diffraction. The beam tilting mode of the SEM (MIRA3 XMU, TESCAN) enabled the determination of the fracture surface topography in 3D [17]. Hence, the crack tip blunting process was characterized by the parameters stretch zone width (SZW) and stretch zone height (SZH).

## RESULTS AND DISCUSSION

### Loading rate dependent crack initiation

Fig. 2 shows the crack growth resistance curves for the different casts under quasi-static and dynamic loading conditions.

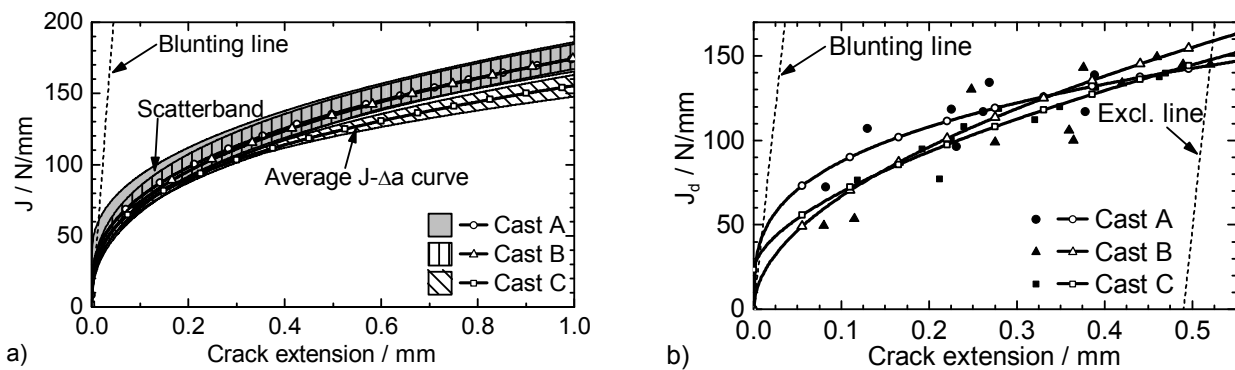


Figure 2: Static (a) and dynamic (b) crack growth resistance curves. No significant difference between different casts due to scattering. Open symbols represent the calculated curves of the type:  $J = A + B(\Delta a)^C$ .

At both loading rates, no significant difference between the different casts was observed. Furthermore, the scattering at the dynamic tests was larger than at quasi-static loading. This was attributed to the testing of multiple specimens under dynamic loading conditions. The increase of loading rate by approximately four orders of magnitude did not result in a considerable deterioration of the toughness behavior. However, a slightly lower toughness was observed at small crack extensions. Furthermore, the slope of the crack growth resistance curve was slightly larger under the dynamic loading conditions. The low sensitivity of the material to the increase of loading rate was attributed to the superposition of two effects: the embrittlement due to the higher strain rate [18] and the decreased flow stress due to adiabatic heating within the plastic zone [19]. These observations are in accordance with Krabiell and Dahl [10], who observed only a slight effect of the loading rate on the fracture toughness at ambient temperature in the case of a quenched and tempered steel.

### Fracture surfaces

Fig. 3 shows the blunting of the crack tip in a region with low inclusion content. The blunting of the precrack was characterized by an intense plastic deformation. Due to the very low content of non-metallic inclusions in this region, void nucleation was inhibited. However, the surrounding area exhibited non-metallic inclusions that nucleated voids.

It can be seen in Fig. 3 that the relatively large amount of non-metallic inclusions in the lower right part of this figure lead to a considerable deviation of the crack path from its original plane. Hence, the agglomeration of non-metallic inclusions favors the crack path deflection at the expense of a minimum area of the fracture surface.

Non-metallic inclusion clusters in the vicinity of the fatigue crack tip resulted in considerable crack path deflection as shown in Fig. 4. Furthermore, crack tip blunting was only observed at regions of the fatigue crack tip that had a distance of at least 50  $\mu\text{m}$  to the inclusion cluster. The deflected crack path was characterized by a nearly flat appearance. This observation can be explained by a shear zone which developed between the original crack (evolved from the fatigue crack) and the voids which formed at the inclusion cluster. These voids coalesced and formed a crack in front of the main crack. It was assumed that these cracks connected analogously to the void sheet mechanism. Hence, no additional void

nucleation was necessary and the strain was localized in a narrow shear zone. Such an effect of non-metallic inclusion clusters was also already observed in the case of tensile loading [20]. In that study, the shear zones were analyzed by means of thermography. Consequently, these zones were detectable by a local increase in heating rate due to localized deformation.

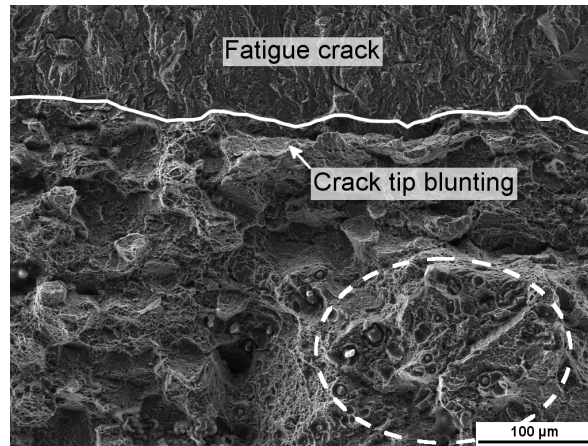


Figure 3: Crack tip blunting in a region with locally low inclusion content. Cast C,  $T = 20\text{ }^{\circ}\text{C}$ , static loading.

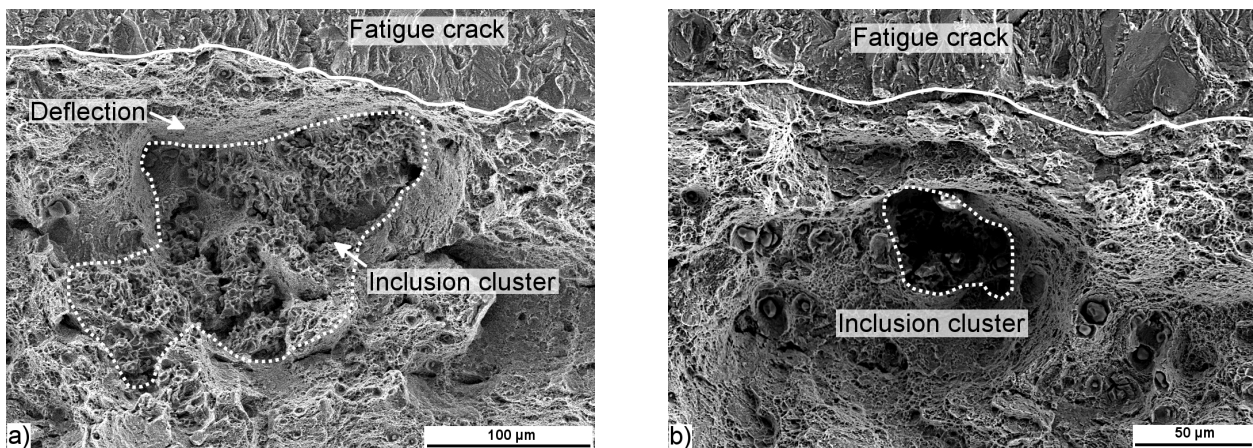


Figure 4: Large non-metallic inclusion cluster directly at the fatigue crack tip. a) Cast A, b) Cast B, dynamic loading.

The amount of crack path deflection was measured by means of stereoscopy enabled by the beam tilting of the SEM. Fig. 5 shows the blunting of the precrack and the deflection due to the non-metallic inclusions.

The observations revealed that crack path deflection superposed the crack tip blunting. The amount of superposition depended on the distance between the inclusion cluster and the fatigue crack tip. Line 1 in Fig. 5b exhibited an intense crack tip blunting due to the distance of approximately  $100\text{ }\mu\text{m}$  between the fatigue crack tip and the cluster. In contrast, line 2 in Fig. 5b exhibited a considerable smaller crack tip blunting due to the smaller distance between the fatigue crack tip and the inclusion cluster. Hence, the characterization of the amount of blunting by the measurement of stretch zone width and stretch zone height can result in erroneous values if only one fracture surface is analysed.

The formation of a shear zone and the crack path deflection was a consequence of the inclusion clusters near the crack tip. Hence, the local decrease of toughness due to the non-metallic inclusions was the reason for the crack path deflection. The crack path deflection, therefore, was not assumed to increase the toughness.

Locally advancing crack fronts can also be found in other materials with non-metallic inclusion. Dynamic loading of a similar G42CrMoS4 in [21] resulted analogously in an inhomogeneous crack front development. Consequently, the crack tip was locally unloaded, which caused an interrupted crack growth. The surrounding material was further loaded and exhibited crack initiation and growth at higher loads.

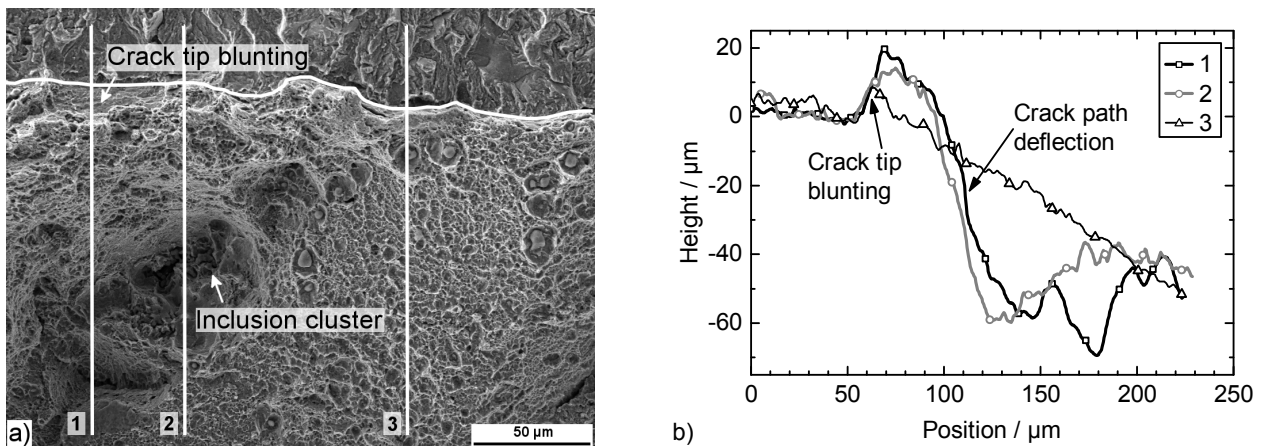


Figure 5: Crack path deflection was considerably larger than crack tip blunting. Cast A, dynamic loading. a) Fracture surface, b) Height profile of the lines shown in a).

### Effect of loading rate

Dynamic loading affected the appearance of the fracture surface. Two typical fracture surfaces are compared in Fig. 6.

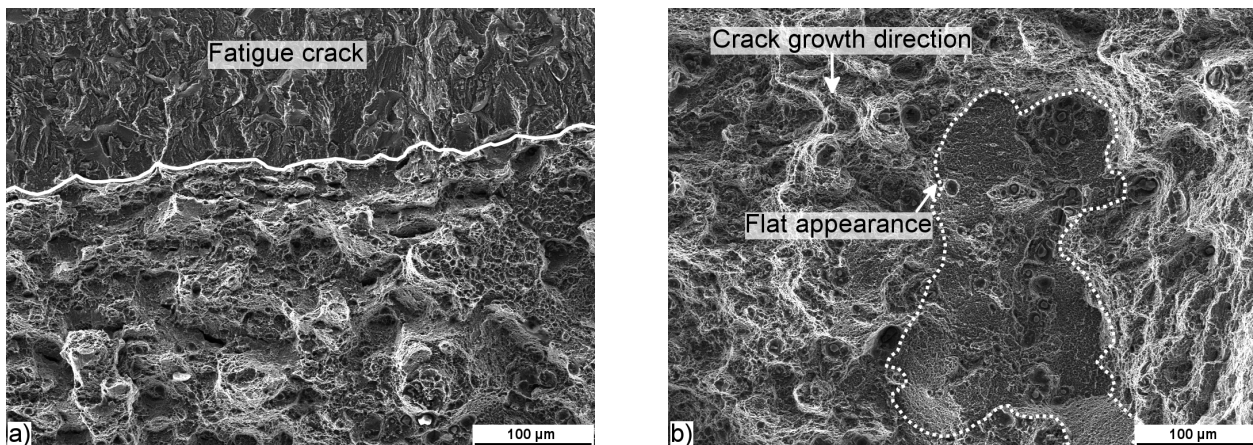


Figure 6: a) Ductile fracture surface, Cast A, static loading; b) flat appearance of ductile fracture surface, Cast C, dynamic loading.

It was observed that the material failed by ductile fracture at both loading rates. However, the dimples in Fig. 6b appeared to be flatter than in Fig. 6a. The inclusion content was nearly equal at that position. Furthermore, it was observed that not only  $\text{Al}_2\text{O}_3$  inclusions but also MnS inclusions influenced the damage evolution. The MnS inclusions found in the regions of the relatively flat fracture surface had a diameter of approximately 5 μm. However, the majority of the small dimples exhibited no measurable non-metallic inclusions. This was attributed to void initiation at small carbides.

## CONCLUSIONS

Intentional addition of non-metallic inclusion was utilized to study the effect of an inhomogeneous inclusion distribution on the formation of the crack path. The effect of clustered non-metallic inclusions was demonstrated in the case of a high-strength cast steel G42CrMo4. The main conclusions can be drawn as follows:

- Clustered non-metallic inclusions significantly affected the crack path. The inclusion clusters promoted the formation of a crack at the weakest point of the cluster. Hence, the main crack was deflected towards the crack in the inclusion cluster.



- Crack path deflection was not considered as a toughness increasing mechanism in the present material. The additionally formed fracture surface due to the crack path deflection did not compensate the detrimental effect of the inclusions regarding toughness.
- The slightly lower crack growth resistance during dynamic tests was attributed to a larger amount of flat-dimpled regions. However, the increase in loading rate by five orders of magnitude did not result in brittle fracture.

## ACKNOWLEDGEMENTS

The authors thank the German Research Foundation (DFG) for its financial support of the investigations at the Collaborative Research Center 920, subproject C05. The support of Georg Maiberg and Sascha Graf was greatly appreciated.

## REFERENCES

- [1] Leslie, W. C., Inclusions and mechanical properties, *Trans. Iron Steel Soc. AIME*, 2 (1983) 1–24.
- [2] Garrison, W. M., Jr., Moody, N. R., Ductile fracture, *J. Phys. Chem. Solids*, 48(11) (1987) 1035–1074. DOI: 10.1016/0022-3697(87)90118-1.
- [3] Braun, T. B., Elliott, J. F., Flemings, M. C., The clustering of alumina inclusions, *Met. Trans. B*, 10(2) (1979) 171–184. DOI: 10.1007/BF02652461.
- [4] Thomson, R. D., Hancock, J. W., Ductile failure by void nucleation, growth and coalescence, *Int. J. Fract.*, 26(2) (1984) 99–112. DOI: 10.1007/BF01157547.
- [5] Beremin, F. M., Cavity formation from inclusions in ductile fracture of A508 steel, *Met. Trans. A*, 12 (1981) 5, 723–731. DOI: 10.1007/BF02648336.
- [6] Cox, T. B., Low, J. R., Jr., An investigation of the plastic fracture of AISI 4340 and 18 Nickel-200 grade maraging steels, *Met. Trans.*, 5 (1974) 1457–1470. DOI: 10.1007/BF02646633.
- [7] Hancock, J. W., Mackenzie, A. C., On the mechanisms of ductile failure in high-strength steels subjected to multi-axial stress-states, *J. Mech. Phys. Solids*, 24(2–3) (1976) 147–160. DOI: 10.1016/0022-5096(76)90024-7.
- [8] Thomason, P. F., Ductile fracture by the growth and coalescence of microvoids of non-uniform size and spacing, *Acta Metall. Mater.*, 41(7) (1993) 2127–2134. DOI: 10.1016/0956-7151(93)90382-3.
- [9] Bourcier, R. J., Koss, D. A., Smelser, R. E., Richmond, O., The influence of porosity on the deformation and fracture of alloys, *Acta Metall.*, 34(12) (1986) 2443–2453. DOI: 10.1016/0001-6160(86)90147-1.
- [10] Krabiell, A., Dahl, W., Zum Einfluß von Temperatur und Beanspruchungsgeschwindigkeit auf die Rißzähigkeit von Baustählen mit unterschiedlicher Festigkeit, *Arch. Eisenhüttenwes.*, 53(6) (1982) 225–230.
- [11] Thomason, P. F., *Ductile fracture of metals*. Oxford: Pergamon Press (1990).
- [12] Yamamoto, H., Conditions for shear localization in the ductile fracture of void-containing materials, *Int. J. Fract.*, 14(4) (1978) 347–365. DOI: 10.1007/BF00015989.
- [13] Zehnder, A. T., Rosakis, A. J., On the temperature distribution at the vicinity of dynamically propagating cracks in 4340 steel, *J. Mech. Phys. Solids*, 39(3) (1991) 385–415. DOI: 10.1016/0022-5096(91)90019-K.
- [14] Emmel, M., Aneziris, C. G., Schmidt, G., Krewerth, D., Biermann, H., Influence of the chemistry of surface functionalized ceramic foam filters on the filtration of alumina inclusions in steel melts, *Adv. Eng. Mater.*, 15(12) (2013) 1188–1196. DOI: 10.1002/adem.201300118.
- [15] Henschel, S., Krewerth, D., Ballani, F., Weidner, A., Krüger, L., Biermann, H., Emmel, M., Aneziris, C. G., Effect of filter coating on the quasi-static and cyclic mechanical properties of a G42CrMo4 casting, *Adv. Eng. Mater.*, 15(12) (2013) 1216–1223. DOI: 10.1002/adem.201300125.
- [16] ISO 12135, 2002: Metallic materials – Unified method of test for the determination of quasistatic fracture toughness.
- [17] Weidner, A., Mottitschka, T., Biermann, H., Henkel, S., Determination of stretch zone width and height by powerful 3D SEM imaging technology, *Eng. Fract. Mech.*, 108 (2013) 294–304. DOI: 10.1016/j.engfracmech.2013.03.021.
- [18] Kußmaul, K., Klenk, A., Link, T., Schüle, M., Dynamic material properties and their application to components, *Nucl. Eng. Des.*, 174 (1997) 3, 219–235. DOI: 10.1016/S0029-5493(97)00134-9.
- [19] Odeshi, A. G., Al-ameeri, S., Bassim, M. N., Effect of high strain rate on plastic deformation of a low alloy steel subjected to ballistic impact, *J. Mater. Process. Tech.*, 162–163 (2005), 385–391. DOI: 10.1016/j.jmatprotec.2005.02.157.



- [20] Henschel, S., Krüger, L., Effect of non-metallic inclusions on the local mechanical behaviour of a G42CrMo4 casting, MATEC Web of Conferences, 12 (2014) 04007. DOI: 10.1051/mateconf/20141204007.
- [21] Krüger, L., Trubitz, P., Henschel, S., Bruchmechanisches Verhalten unter quasistatischer und schlagartiger Beanspruchung. In: H. Biermann and L. Krüger (Eds.): Moderne Methoden der Werkstoffprüfung. Weinheim: Wiley-VCH, (2014) 1–52.